Article

Not peer-reviewed version

Effect of Copper Doping on the Structural, Electrical, and Magnetic Properties of Mg-Co Ferrites

Kuswanth S *, Kavyasri D , Mahesh P , Rao M P , Samatha K

Posted Date: 28 March 2024

doi: 10.20944/preprints202403.1642.v2

Keywords: Cu-doped Mg-Co ferrites; Solid-state reaction method; Structural characterization; Morphological characterization; Magnetic properties; DC-Electrical resistivity; Magnetic storage devices; High-frequence

Article

Effect of Copper Doping on the Structural, Electrical, and Magnetic Properties of Mg-Co Ferrites

Kuswanthkumar S *, Kavyasri D, Mahesh P, Rao M P and Samatha K

Department of Physics, Andhra University, Waltair, Visakhapatnam, Andhra Pradesh, IN 530003; kavyasri27.degala@gmail.com (K.D.); maheshpeyyala18@gmail.com (M.P.); raomp17@gmail.com (R.M.P.); samatha_k2002@yahoo.co.in (S.K.)

* Correspondence: kuswanthkumar@gmail.com; Tel.: +91 9493026949

Abstract: This research paper focuses on the synthesis and characterization of Cu-doped Mg-Co ferrites with varying compositions ($Mg_{0.6-x}Co_{0.4}Cu_xFe_2O_4$, where x = 0.0, 0.1, 0.2, and 0.3) using a solid-state reaction method. This paper also investigates the structural, morphological, magnetic, and electrical characteristics of synthesized $Mg_{0.6-x}Co_{0.4}Cu_xFe_2O_4$, where x = 0.0, 0.1, 0.2, and 0.3. The X-ray diffraction (XRD) technique confirms the ferrites spinel structure in the Fd-3m space group, with average crystallite sizes ranging from 57.29 to 48.57 nm. Fourier Transform Infrared (FTIR) spectroscopy verifies chemical and structural changes, while scanning electron microscopy (SEM) reveals cubic crystal growth with an average grain size of 1 to 1.5 μm. DC electrical resistivity decreases with increasing temperature and Cu^{2+} substitution, ranging from 1.4 x 10^6 Ω-cm to 6.7 x 10^5 Ω-cm. The study suggests a correlation between resistivity and Cu^{2+} concentration. Magnetic behavior, studied using a Vibrating Sample Magnetometer (VSM), shows dependence on dopant concentration, with coercivity ranging from 157 Oe to 256 Oe. The results indicate potential applications in magnetic storage devices, antennas, transformers, and high-frequency electronics.

Keywords: Cu-doped Mg-Co ferrites; solid-state reaction method; structural characterization; morphological characterization; magnetic properties; electrical resistivity; magnetic storage devices; high-frequency electronics

1. Introduction

Ferrites are the class of materials having general formula, MFe_2O_4 (M = divalent metal ions; examples include Mg, Zn, Ni, Co, etc.). Depending on their structure, composition and morphology, ferrites exhibit interesting optical, magnetic, and electrical properties which make them a suitable candidate for applications in various fields [1]. Among various ferrite materials, magnesium ferrite ($MgFe_2O_4$) is one such important ferrite material having a spinel structure with inversion mode. In normal spinel ferrite, divalent metal ions and trivalent metal ions occupy tetrahedral and octahedral sites respectively [2]. In inverse spinel ferrites, maximum trivalent ions occupy tetrahedral sites, and the remaining trivalent and divalent ions occupy octahedral sites [3]. Ferrites can be doped with additional metal ions, and each additional metal ion affects the chemical formula and physical and chemical properties of the material [4].

Magnesium ferrite due to its high curie temperature, high saturation magnetization, and low coercivity is called soft ferrite and is commonly utilized in high-frequency electronic devices and microwave applications, etc. [5]. Cobalt ferrite ($CoFe_2O_4$) has an inverse spinel structure and due to its higher coercivity than Mg ferrite, it is also known as a hard ferrite [6]. Cobalt doping improves the coercivity of magnesium ferrite. Additionally, a unit cell of magnesium ferrite shrinks because of cobalt's lower ionic radius [7]. In comparison to other ferrites, Mg-Co ferrite has a high coercivity, moderate saturation magnetization, strong chemical stability, high mechanical hardness, and inexpensive production costs. It is also known as a good candidate for nuclear magnetic resonance and as a photocatalyst. By doping additional metal ions into Mg-Co ferrite, different magnetic materials can be synthesized with unique structures, physical and chemical properties. Metal-doped

 doi:10.20944/preprints202403.1642.v2

magnesium cobalt ferrites have gained attention due to their exceptional electrical and magnetic properties, making them ideal for high-frequency applications [8], such as in the fabrication of transformers where they are integral in reducing signal noise and enhancing signal quality. These materials can also be used in the development of highly sensitive magnetic sensors for applications like automotive and industrial sensing.

Ferrite cores are crucial in Sound Detection and Ranging (SODAR) pre-amplifiers for significantly reducing signal noise, enhancing the accuracy and reliability of environmental monitoring. These cores, made from magnesium and cobalt ferrites, are selected for their high saturation magnetization and custom-tailored coercivity. By doping these ferrites with specific metals like cobalt to boost coercivity or copper to modify electrical properties, their effectiveness in suppressing electromagnetic interference is maximized [9]. This reduction of noise signals is essential for improving the fidelity of sound wave detection and analysis in SODAR systems, demonstrating the unique application of ferrite materials in high-frequency and noise-sensitive technologies, where signal clarity and noise reduction are critical.

The effectiveness of ferrite cores in suppressing electromagnetic interference (EMI) in cables and wires, which is analogous to their role in SODAR systems, has been thoroughly investigated [10,11]. Additionally, advancements in the performance of sense-amplifier circuits through pre-amplification strobing and noise-matched clipping further highlight the technological importance of minimizing noise for enhanced signal clarity [12]. The prediction and analysis of the noise reduction effect of ferrite beads on electromagnetic emission from digital PCBs also provides insight into the broader applications of ferrites in EMI suppression [13].

The present study reports the synthesis of Cu^{2+} ions substituted Mg-Co ferrites ($Mg_{0.6-x}Cu_xCo_{0.4}Fe_2O_4$ with x = 0.0, 0.1, 0.2, and 0.3) by a solid-state reaction method and evaluate the effect of Cu^{2+} substituting on the structural, dc electrical, and magnetic properties of magnesium-cobalt ferrite and to find a correlation between them. The solid-state method, widely used in materials science, involves directly reacting powdered reactants at high temperatures. It offers simplicity, cost-effectiveness, and the production of phase-pure products. This method enables thorough mixing at the atomic level, resulting in homogeneous and finely divided products. Different synthesis processes have specific advantages and considerations, emphasizing the importance of selecting the appropriate method based on desired characteristics, scalability, and application requirements. Solid state synthesis offers precise control over crystallinity and phase purity, making it suitable for applications needing accurate stoichiometry and well-defined crystal structures.

The structural and morphological properties of the synthesized $Mg_{0.6-x}Cu_xCo_{0.4}Fe_2O_4$ have been investigated by using standard characterization techniques. DC electric resistivity of synthesized ferrite material has been evaluated by a two-probe method and the magnetic measurement has been done using a Vibrating sample magnetometer (VSM). The results of this comprehensive study suggest that the frequency magnetic and electronic device applications, including those in Sound Detection and Ranging (SODAR), offering advancements in signal quality and noise reduction in such sophisticated technologies.

It's pertinent to note that while this investigation seeks to improve ferrites noise reduction capabilities in SODAR applications, it specifically concentrates on the effects of Cu^{2+} ion substitution within a defined range. The findings of this research are primarily applicable to the development and application of ferrite cores in SODAR amplifier systems. Future studies could extend this scope to include other doping elements and investigate their impact on ferrite properties, potentially paving the way for new applications of ferrite materials in high-frequency and noise-sensitive technologies.

2. Materials and Methods

2.1. Chemicals

High-purity analytical grade (A.R) chemicals of transition metal oxides were used for standard ceramic synthesis. Magnesium Oxide (MgO ≥99.99%), Ferric oxide (Fe_2O_3 ≥99.99%), Copper oxide (CuO ≥99.99%), Cobalt (II) oxide (CoO ≥99.99%) were purchased from Himedia. Acetone (C_3H_6O),

 doi:10.20944/preprints202403.1642.v2

Potassium Bromide (KBr), Silver (Ag), and Poly Vinyl Alcohol $(C_2H_4O)_x$ were purchased from Merck. All the chemicals were used without further purification.

2.2. Synthesis of Cu^{2+} Substituted Mg-Co Ferrites

Cu^{2+} substituted $Mg_{0.6-x}Cu_xCo_{0.4}Fe_2O_4$(x = 0.0, 0.1, 0.2, and 0.3) were prepared by the solid-state reaction method. Analytical grade oxides MgO, Fe2O3, CuO, and CoO, were taken in stoichiometric proportions and grounded for 6 h in an agate motor and pestle to obtain in powder form. The powder is then calcined at 900 °C for 4 h. After mixing a few drops of PVA as a binder, the calcined samples are pressed to a disk-shaped pellet under a pressure of 7 tons per 5 minutes and sintered at 1200 °C for 4 h in the air at the rate of 5 °C/min. The pellet's surfaces are polished carefully, washed with acetone, and coated with silver paste for use as electrodes. Figure 1 shows the schematic of the synthesis process of Cu-doped magnesium-cobalt ferrites. The prepared samples were used for further characterization.

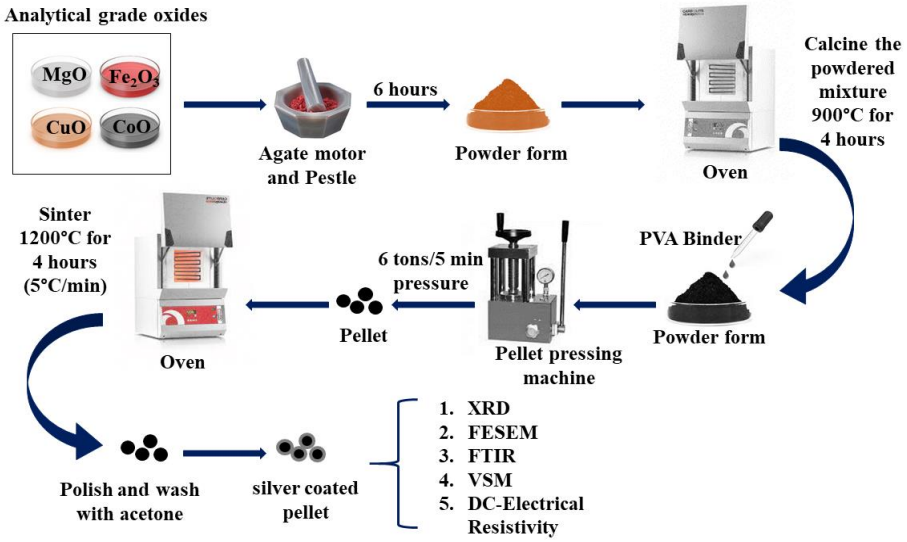

Figure 1. Schematic representation of the synthesis process of Cu-doped Mg-Co Ferrites.

2.3. Characterizations

2.3.1. Structural Characterizations

The identification of phase formation of synthesized magnesium ferrite powder samples was done on a PANalytical XPERT-PRO diffractometer fitted with Cu Kα radiation (λ = 1.54060 Å) at the scan rate of 2 °/min in the 2θ range of 10 to 80 degrees. The observations were recorded at 40 mA and 45 kV. The experimental XRD patterns of the synthesized samples were matched with the standard reference data card from the Joint Committee on Powder Diffraction Standards (JCPDS) or the International Center of Diffraction Data (ICDD).

The chemical and structural changes are verified by FTIR spectrometer (IR Prestige21 Shimadzu). The synthesized ferrite powdered samples were mixed with solid potassium bromide (KBr), grounded, and then pressed in a standard hydraulic press to form a spherical shape pellet for measurements. The spectra of all the synthesized samples were collected in the range of 200-4000 cm^{-1} at room temperature.

2.3.2. Morphological and Elemental Characterization

The microstructure and morphology of the synthesized magnesium ferrite samples were measured by Field Emission Scanning Electron Microscope (Carl Zeiss, EVO MA 15, Oxford Instruments, Inca Penta FETx3.JPG equipment) operating at 30 kV. Grain size measurement from the electron micrographs was performed using image processing software ImageJ version 1.53e, which

 doi:10.20944/preprints202403.1642.v2

is a public domain Java-based image processing program developed at the National Institutes of Health, USA [14].

2.3.3. Magnetic Measurements

The Vibrating Sample Magnetometer (Lakeshore 735) was used to measure the magnetization behaviour of the synthesized ferrite samples. Finely powdered samples of synthesized ferrites (approximately 125 mg each) were carefully mounted on the Vibrating Sample Magnetometer (Lakeshore 735) holder. To ensure correct alignment within the magnetic field of the VSM, the samples were isolated from other metallic components to prevent any interference. An external magnetic field at a magnetic field strength of 1Tesla was applied, and the magnetization of the vibrating samples was recorded, producing a hysteresis loop. All the measurements were conducted at room temperature to maintain stability, as temperature fluctuations could alter magnetization behaviour. Following measurements, data analysis was performed to identify key magnetic properties: coercivity, remanence, and saturation magnetization. Rigorous calibration of the VSM was maintained throughout, with thorough cleaning post-use to prevent contamination.

2.3.4. DC Electrical Resistivity

The DC electrical resistivities of the synthesized magnetic ferrite samples were determined for conductivity investigation by using a two-probe method and measured between the temperatures of 303K and 873 K. The sample in the form of a pellet was held between two electrodes. The silver paste was applied on both surfaces of the pellet to ensure good ohmic contact. The current and voltage measurements were carried out during rising temperatures. The temperature of the sample was measured using a chrome-aluminum thermocouple.

3. Results and Discussion

3.1. Identification and Interpretation of Crystal Structure by X-ray Diffraction (XRD) Analysis

The crystal structure, phase purity, and structural parameters of the synthesized samples were confirmed by analyzing their XRD patterns. Figure 2 shows the X-ray diffraction patterns of the synthesized samples. XRD patterns with the corresponding (hkl) planes; (111), (220), (311), (400), (422), (511), and (440) were observed for all the samples. The XRD patterns were well matched with the standard diffraction patterns of cubic spinel structure with the space group Fd3m for all the samples (JCPDS card no. 73-1720 and 22-1086) [15]. All the reflections are broader than those for samples of ceramic. The presence of broader peaks suggests that the size of the synthesized ferrite particles is small. No impurity peaks were observed. The XRD result confirms the synthesis of Cu^{2+}ions substituted magnesium ferrites with phase purity and small crystallite size [16].

 doi:10.20944/preprints202403.1642.v2

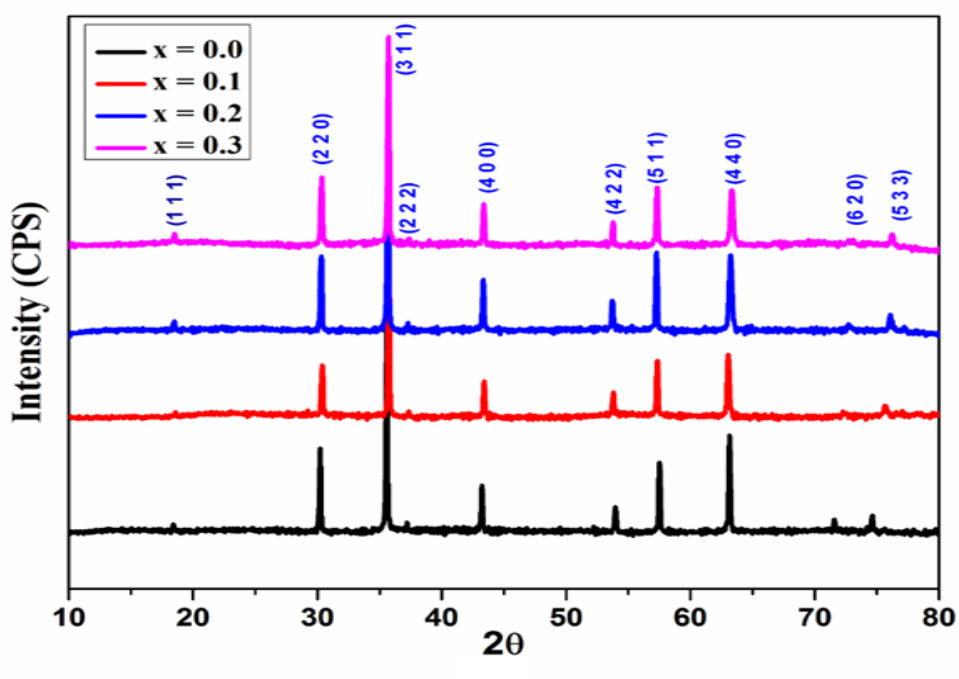

Figure 2. X-ray diffraction patterns of $Mg_{0.6-x}Cu_xCo_{0.4}Fe_2O_4$ (x = 0, 0.1, 0.2, and 0.3).

The lattice constants of the synthesized samples were calculated by using the equation below (equation (1)) and the values of lattice constant(a) for the synthesized ferrite samples are reported in Table 1 below.

$$a = d \times \sqrt{(h^2 + k^2 + l^2)} \quad (1)$$

where, d is the inter-planar spacing and (h k l) are Miller indices of a cubic crystal plane.

Table 1. Lattice constant and Crystallite size of $Mg_{0.6-x}Cu_xCo_{0.4}Fe_2O_4$ (x = 0, 0.1, 0.2, and 0.3).

Parameters	x = 0.0	x = 0.1	x = 0.2	x = 0.3
Lattice constant a (Å)	8.3720	8.3828	8.3614	8.3912
V_{cell} (Å^3)	586.79	589.07	584.57	590.84
Crystallite size (nm)	57.29	51.32	49.91	48.57

The value of the lattice constant values in the samples show irregular changes with different levels of substitution x, in the compound. Specifically, the lattice constant grows when x, changes from 0.0 to 0.1, suggesting that the unit cell might be expanding. However, it decreases at x=0.2 hinting at a decrease in the space between atoms. Then, it grows again at x=0.3. These changes at different substitution levels indicate modification in the distance and interactions between atoms in the crystal, which can significantly affect the material's properties.

The introduction of Cu^{2+} ions, which have a larger ionic radius (0.72 Å) than Mg^{2+} ions (0.65 Å) [17], could be causing these changes in the lattice constant. This might also be related to the presence of Fe^{2+} ions, which have a larger radius (0.78 Å) than Fe^{3+} ions (0.64 Å). The differences in ionic sizes, along with changes in the shape and internal stress in the lattice, are likely causing the lattice constant to increase.

The average crystallite sizes ($D_{(311)}$) of the synthesized Cu doped Magnesium-Cobalt ferrite samples were determined by using the Debye-Scherer formula (equation 2):

$$D = \frac{K\lambda}{\beta \cos\theta} \quad (2)$$

 doi:10.20944/preprints202403.1642.v2

Where D is the average crystallite size, β is the Full width at half maximum of the most substantial reflection in radians, θ is an angle corresponding to the peak position, λ is the wavelength of x-ray radiation which is equal to λ=1.5406 Å, and K is the shape factor of average crystallite, and its value is ~ 0.9.

The values of crystallite sizes for the synthesized ferrites samples are shown in Table 1, which are in good agreement with earlier research [18]. The average crystallite sizes were found in the ranges between 57.29 to 48.57 nm, and the trend of this change is consistent with variations in the lattice constant as shown in Table1. The plot of lattice constant (a) and crystallite size with Co content (x) is shown in Figure 3. The crystallite size has a random value due to the randomness in the cation distribution and sintering condition [19].

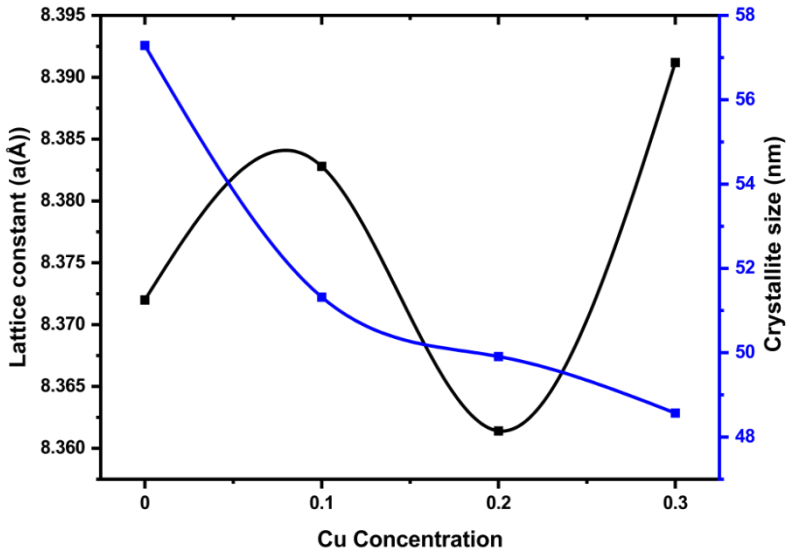

Figure 3. The plot of lattice constant and crystallite size of $Mg_{0.6-x}Cu_xCo_{0.4}Fe_2O_4$ (x = 0.0, 0.1, 0.2, and 0.3.

Average crystallite size is found in the ranges between 57.29 to 48.57 nm calculated using the Debye-Scherrer equation.

3.2. Fourier Transformed Infrared (FTIR) Spectroscopy

The infrared spectra of Cu^{2+} substituted $Mg_{0.6-x}Cu_xCo_{0.4}Fe_2O_4$ with x = 0.0, 0.1, 0.2, and 0.3 samples are shown in Figure 4. Two absorption bands, ν1 and ν2, were observed which lie between 600 and 400 cm^{-1}. These bands correspond to the lower and higher frequencies of the tetrahedral and octahedral metal-oxygen vibration respectively [20]. These bands were found in the wave number range as listed in Table 2. With increasing Cu2+ ion concentration, the value of ν1 is found within the range of 572.88 – 582.52 cm^{-1} and values of ν2 in the range of 401.56 - 407.96 cm^{-1}. The variation in the band positions is due to the cation distribution. These band positions are in good agreement with the previous reports on spinel ferrites [21].

 doi:10.20944/preprints202403.1642.v2

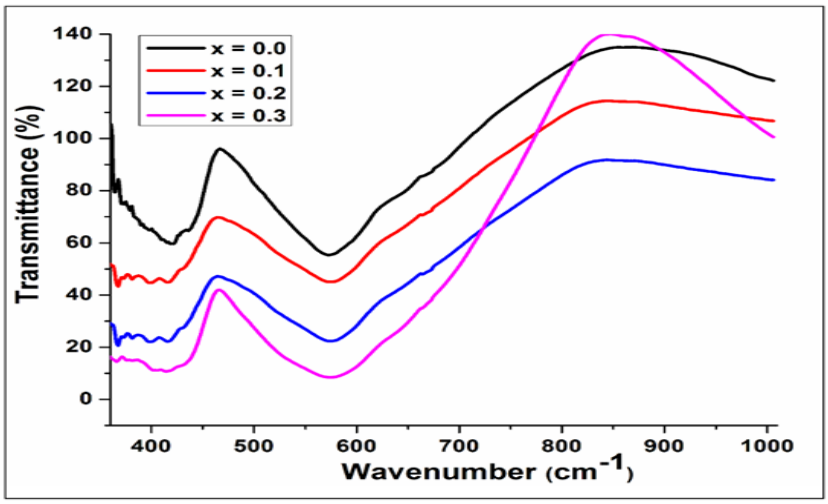

Figure 4. Fourier transform infrared spectra of $Mg_{0.6-x}Cu_xCo_{0.4}Fe_2O_4$ (x = 0, 0.1, 0.2, and 0.3).

Table 2. Wave number value of Cu doped $Mg_{0.6-x}Cu_xCo_{0.4}Fe_2O_4$ (x = 0, 0.1, 0.2, and 0.3).

Composition (x)	x = 0.0	x = 0.1	x = 0.2	x = 0.3
Tetrahedral υ_1 (cm^{-1})	572.88	574.81	579.63	582.52
Octahedral υ_2 (cm^{-1})	410.24	407.96	406.03	401.56

3.3. Assessment of Morphology Using Scanning Electron Microscopy (SEM)

SEM micrographs of the Cu^{2+} substituted $Mg_{0.6-x}Cu_xCo_{0.4}Fe_2O_4$ with x = 0.0, 0.1, 0.2, and 0.3 are presented in Figure 5. The micrograph shows the growth of regular cubic crystals with the average grain size determined by using Image J software, ranging from 1 to 1.5 μm, depending on the substitution of Cu^{2+}. The microstructure of synthesized ferrite samples is significantly impacted by copper because it makes the liquid phase sintering easier. Moreover, the driving force for grain boundary movement and the restraining force produced by pores can be thought of as competitors in the process of grain growth [22]. The force generated by the thermal energy during sintering causes grain boundaries to cover pores, reducing the volume of the pores and increasing the density of the material. The uniform distribution of grain size occurs if the driving force acting on each grain is homogeneous. The non-homogeneous driving force on the grains in the current investigation is the cause of the non-uniformity of grain size [23]. The observed microstructures of synthesized materials give them suitable electromagnetic properties like permeability and magnetization.

 doi:10.20944/preprints202403.1642.v2

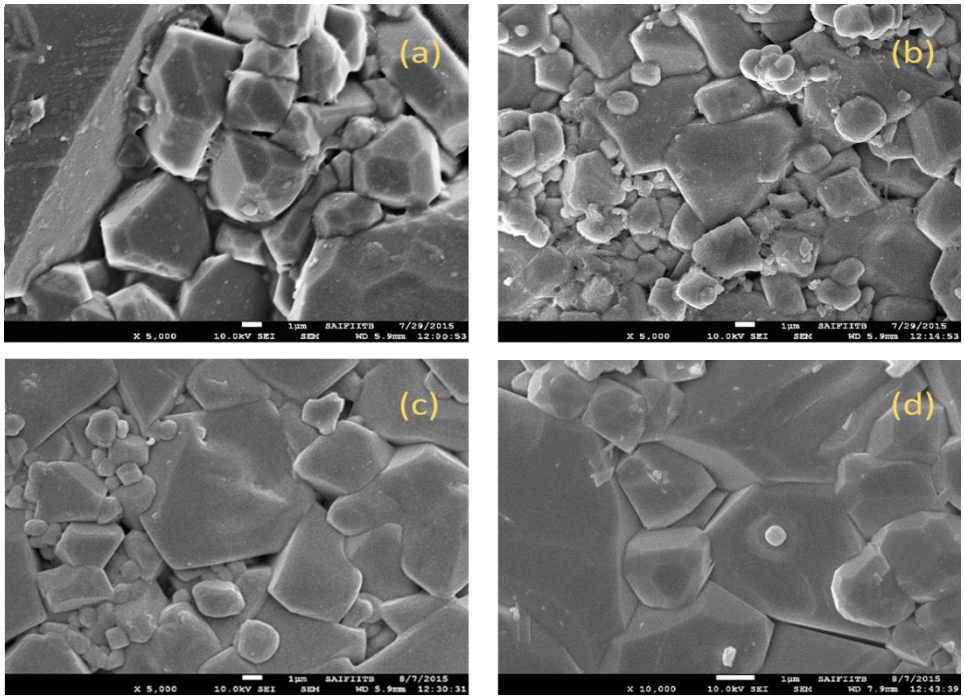

Figure 5. SEM micrographs of $Mg_{0.6-x}Cu_xCo_{0.4}Fe_2O_4$ with(a) x = 0, (b) x = 0.1, (c) x = 0.2, and (d) x = 0.3.

Synthesized ferrites show the growth of regular cubic crystals with average grain size ranges from 1 to 1.5 μm, depending on the substitution of Cu^{2+}

3.4. Magnetic Measurements

The magnetic measurements were done using a vibrating sample magnetometer (VSM), to determine the values of saturation magnetization, and coercivity of the Cu^{2+} substituted $Mg_{0.6-x}Cu_xCo_{0.4}Fe_2O_4$ (x = 0.0, 0.1, 0.2, and 0.3) at a magnetic field strength of 1T at room temperature. Figure 6 shows the plotted M-H curve of saturation magnetization against the applied magnetic field for different concentrations of synthesized ferrites samples. It is clear from the figure that magnetization increases with the applied magnetic field.

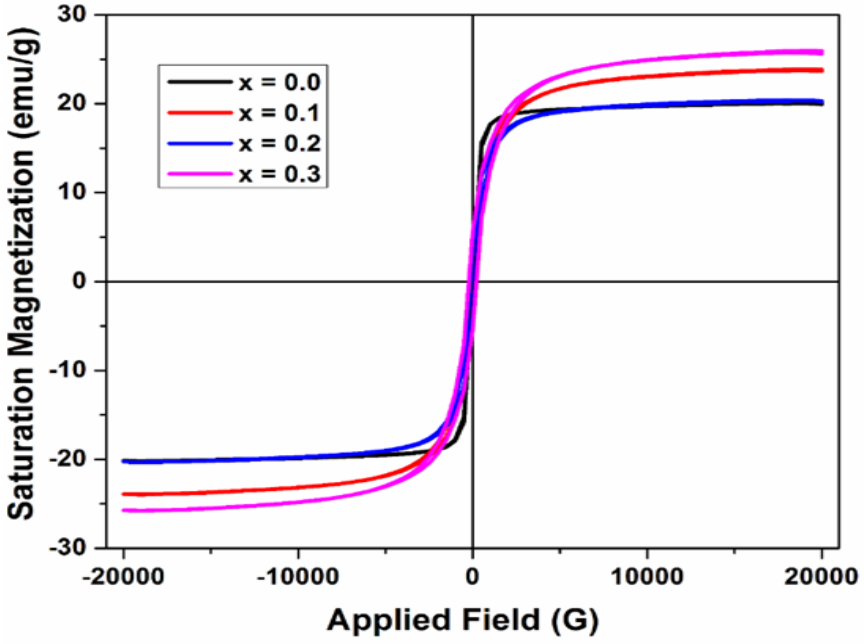

Figure 6. Magnetic Hysteresis loops of $Mg_{0.6-x}Cu_xCo_{0.4}Fe_2O_4$ (x = 0, 0.1, 0.2, and 0.3).

 doi:10.20944/preprints202403.1642.v2

The saturation magnetization (Ms) and coercivity (Hc) of synthesized ferrite samples were obtained from the hysteresis loops as shown in Figure 6 and their values are listed in Table 3 below. It was observed that the value of saturation magnetization (M_s) first increased and then decreased with the increasing dopant (Cu^{2+}) concentration. The coercivity was found to depend on Cu^{2+} concentration and ranges from 157 Oe to 256 Oe. This result is consistent with the previous studies, which showed the magnetic properties are enhanced due to the cation substitution. In a study, Hoyos-Sifuenteset al. have reported the synthesis of magnesium ferrite material ($MgFe_2O_4$) and a M_s value of 17 emu/g [24]. Balavijayalakshmiet al.,in their work synthesized the cobalt substituted magnesium ferrites andreported an increase in saturation magnetization (M_s), remanent magnetization (M_r) and coercivity (H_c) as the concentration of cobalt substitution increases,attributed to the change in the concentration of cation distribution [25].Thus, the excellent magnetic behavior of the synthesized Cu-doped Mg-Co ferrites can be used for high frequency magnetic storage device applications.

Table 3. Magnetization and coercivity values for $Mg_{0.6-x}Cu_xCo_{0.4}Fe_2O_4$.

Parameters	x = 0.0	x = 0.1	x = 0.2	x = 0.3
Magnetization M_s [emu/g]	19.95	23.68	20.30	25.64
Coercivity H_c (Oe)	157	266	256	193

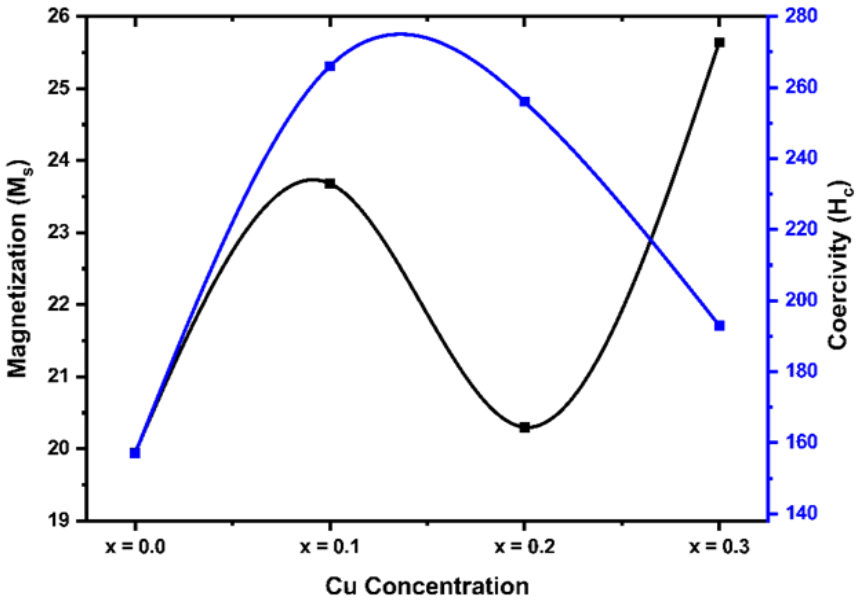

Figure 7. Variation of saturation magnetization (M_s) and coercivity (H_c) with Cu content for $Mg_{0.6-x}Cu_xCo_{0.4}Fe_2O_4$.

Neel's model can explain the observed magnetic behaviour of the Cu-substituted Mg-Co ferrites samples. The saturation magnetization, and coercivity, of a ferrite depends on its cation occupancy, composition, microstructure, and density. Neel's two-sublattice model states that the magnetic moment per formula unit is given by the difference between the magnetic moments of each sublattice. The total magnetization value can be obtained by their differences:

$M = |M_B - M_A|$

Where M_A and M_B are the A and B sublattice's magnetic moments per formula unit respectively in μB (Bohr magneton).

From Table 3, the observed variation in saturation magnetization, i.e., first increase and then decrease with the increasing dopant (Cu^{2+}) concentration, indicates the fluctuation in the cationic distribution in the two interstitial sites; tetrahedral (A) and octahedral (B) [26]. With the substitution

 doi:10.20944/preprints202403.1642.v2

of Cu^{2+} on the B site, the reduction in B-site magnetization causes a decrease in the ferrite's magnetization value (M_s), and this substitution of Cu^{2+} ions into the B-sites will promote the migration of Fe^{3+} ions into the A-site, which then increase magnetization of A-site.

The different exchange interactions, such as A-B, A-A, and B-B, which depend on the distribution of magnetic and non-magnetic ions at the A and B sites, can also be used to explain the variations in M_s value. The B-B and A-A interactions are known to be subordinate to the A-B interaction, which is the strongest. As the Cu level increased, the iron ions moved to the A site, exhibiting less A-B interaction with iron on the B site and thus the ferromagnetic behaviour decreased with increasing Cu^{2+} concentration. Moreover, the coercivity first increased and then decreased due to the greater anisotropic constant of the Cu^{2+} substituted Mg-Co ferrites, which is completely related to the bulk density of the samples. This result indicates that samples with high coercivity can be utilized for applications in microwave absorption systems, switch-mode power supplies, MLCIs, and dc-dc converters.

3.5. DC Electrical Resistivity Studies

The prepared pellets of the synthesized samples were examined by two probe methods to determine the resistivity of Cu^{2+} substituted $Mg_{0.6-x}Cu_xCo_{0.4}Fe_2O_4$ with x = 0.0, 0.1,0.2, and 0.3 samples in the range 300K - 873K. The temperature of the sample was measured using a chrome-alumni thermocouple. The resistivity of the sample is obtained by using equation (3) below:

$$\varrho = R_b A/L \tag{3}$$

R_b is the resistance of the sample, A is the surface area of the sample and given by πr^2, r is the radius of the sample pellet, and L is the thickness of the sample.

The plot of log ϱ against 1/T is shown in Figure 8. The graph obeys the Arrhenius relation (equation (4)), showing the semiconducting behavior of synthesized samples [27].

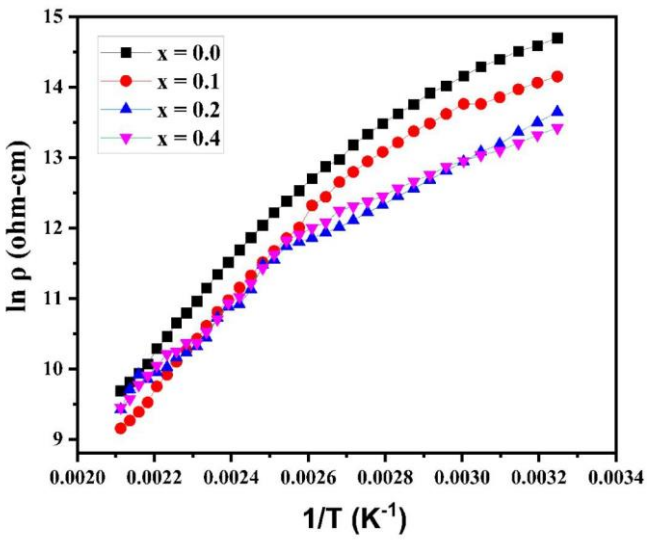

Figure 8. Plots of DC electrical resistivity of various $Mg_{0.6-x}Cu_xCo_{0.4}Fe_2O_4$.

$$\rho = \rho_o \exp(\Delta E/kT) \tag{4}$$

Where k is the Boltzmann constant, T is the absolute temperature, ΔE is the activation energy for conduction, ρ_o is resistivity at 0K, and ρ is the resistivity of the material at TK.

It is clear from the variation of electrical resistivity (logϱ) with temperature (1/T) curves (at different Cu^{2+} concentrations) that each plot adheres to the Arrhenius relation. The resistivity of ferrite samples (at different Cu^{2+} concentrations) reduces as the temperature rises, showing that the samples are semiconducting. The DC electrical resistivity was maximum with a value of ~ 2.4×10^6 without

 doi:10.20944/preprints202403.1642.v2

copper substitution in magnesium-cobalt ferrite samples. With the copper substitution, the electrical resistivity was calculated and found to decline from 1.4 x 10^6 Ω-cm (for x = 0.1) to 6.7 x 10^5 Ω-cm (for x = 0.3). It shows that with the increase in Cu cation concentrations synthesized ferrite samples show a decrease in the resistivity. The smaller grain size is responsible for the greater resistivity value. Large numbers of grain boundaries found in smaller grains serve as sites for scattering the flow of electrons, thus raising the resistivity.Bharathi et al. in a study, reported the temperature dependent dc electrical resistivity and a semiconducting behaviour of synthesized Cu^{2+} substituted Mg-Co ferrite [28].This result is consistent with our study, which showed the decrease in electrical resistivity dependent on temperature and cation substitution and semiconducting nature of synthesized copper-doped Mg-Co ferrites.

The activation energy plot of samples against Cu^{2+} concentration is shown in Figure 9, where the concentration content decreases the activation energy and samples' resistivity due to the hopping mechanism [29]. The activation energy values for $Mg_{0.6-x}Cu_xCo_{0.4}Fe_2O_4$ (x = 0, 0.1, 0.2, and 0.3) is shown in Table 4.

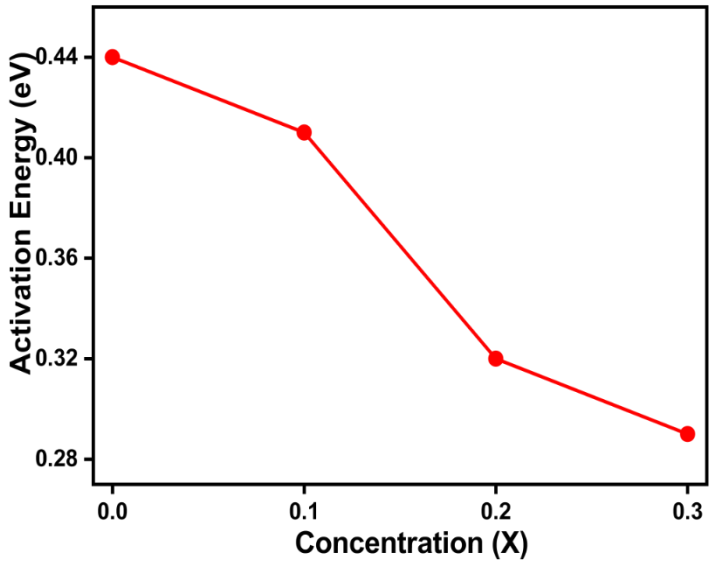

Figure 9. Various activation energy with Cu content for $Mg_{0.6-x}Cu_xCo_{0.4}Fe_2O_4$.

Table 4. Activation energy values for $Mg_{0.6-x}Cu_xCo_{0.4}Fe_2O_4$ (x = 0, 0.1, 0.2, and 0.3).

Parameters	x = 0.0	x = 0.1	x = 0.2	x = 0.3
Activation Energy (eV)	0.430	0.408	0.386	0.362

The electrical conduction in ferrites with Cu^{2+} ions is due to the electron jumping (or) hopping between Fe^{2+} to Fe^{3+} on the adjacent octahedral sites (B-sites) of the ferrite structure. When the sintering of samples is done at high temperatures, the conversion of Fe^{3+} ions to Fe^{2+} ions create oxygen vacancies for maintaining the spinel lattice's neutrality. The result of this study is consistent with a previous report, where Parajuli et al. synthesized magnesium substituted copper-cobalt ferrites and reported their electrical properties and the activation energy based on the hopping mechanism [30].

4. Conclusion

This study successfully synthesized Cu2+ substituted Mg-Co ferrites (Mg0.6-xCuxCo0.4Fe2O4 with x values of 0.0, 0.1, 0.2, and 0.3) using a solid-state reaction method, showcasing the effective incorporation of copper into the ferrite structure. The resulting materials displayed a single-phase

 doi:10.20944/preprints202403.1642.v2

cubic spinel structure across all samples, as confirmed by XRD analysis. This structural integrity is crucial for applications requiring precise magnetic and electrical properties. Incorporating larger Cu2+ ions increased the lattice constant, highlighting the impact of ionic substitution on the ferrite's crystal structure. SEM revealed uniformly sized cubic crystals, with grain sizes ranging from 1 to 1.5 μm, indicating a homogeneous synthesis process. Further structural confirmation came from FTIR, where the observed absorption bands aligned with the characteristic metal-oxygen vibrations in tetrahedral and octahedral sites, consistent with spinel ferrites. These Cu-doped ferrites' electrical resistivity and magnetic properties showed significant variation with the level of Cu2+ substitution. A decrease in electrical resistivity with increasing Cu2+ content suggests enhanced electrical conductivity, making these materials suitable for applications with desirable lower resistivity and semiconducting behavior. Specifically, the reduction in activation energy for electrical conductivity with higher Cu2+ concentration improves the efficiency of high-frequency electronic devices. Magnetic measurements revealed increased saturation magnetization and coercivity with Cu2+ concentration, indicating the potential for tailored magnetic properties in device applications.

The relevance of these findings extends to the application of ferrites in SODAR systems. The synthesized materials, with their high DC electrical resistivity and adjustable coercivity, offer promising prospects for enhancing signal quality and noise reduction in such sophisticated technologies. In SODAR pre-amplifiers, where signal clarity and noise suppression are paramount, Cu-doped Mg-Co ferrites' tailored magnetic and electrical properties could significantly improve environmental monitoring accuracy and reliability. This study not only underscores the versatility of ferrites in high-frequency and noise-sensitive applications but also paves the way for future research into other doping elements to further expand the application scope of ferrite materials in advanced technological systems.5. Patents: This research has not resulted in any patents

Author Contributions: Kuswanthkumar S conceptualized the study, contributed to methodology, validation, data curation and created the visualizations and graphical representations of the research data. Kuswanthkumar S and Kavyasri D drafted the initial version of the manuscript based on the research findings and revised and refined the manuscript through multiple rounds of editing. Mahesh P and Samatha K managed the allocation of research materials and equipment. Rao M P provided guidance and oversight throughout the research work.

Funding: This research received no external funding.

Institutional Review Board Statement: Not applicable.

Informed Consent Statement: Not applicable.

Data Availability Statement: The authors declare that the data supporting the findings of this study are available within the article. No new data were created or analyzed in this study.

Conflicts of Interest: The authors declare no conflicts of interest.

References

1. Reddy, D. H. K. and Yun, Y. S., 2016: Spinel ferrite magnetic adsorbents: Alternative future materials for water purification, Coordination Chemistry Reviews, 315, 90, https://doi.org/10.1016/j.ccr.2016.01.012
2. Chandramouli, K., Rao, P. A., Suryanarayana, B., Raghavendra, V., Mercy, S. J., Parajuli, D., Taddesse, P., Mulushoa, S. Y., Mammo, T. W. and Murali, N., 2021: Effect of Cu substitution on magnetic and DC electrical resistivity properties of Ni–Zn nanoferrites, Journal of Materials Science: Materials in Electronics, 32, 15754–15762, https://doi.org/10.1007/s10854-021-06127-7
3. Mahmoud, W. E., Shams, M., and Ali, M. F., 2016: Magnetic properties of spinel ferrites synthesized by sol-gel method, Journal of Magnetism and Magnetic Materials, 400, 38-46. https://doi.org/10.1016/j.jmmm.2015.08.089
4. Eltabey, M. M., Massoud, A. M., and Radu, C., 2014: Microstructure and superparamagnetic properties of Mg-Ni-Cd ferrites nanoparticles, Advances in Materials Science and Engineering, Article ID 492832, https://doi.org/10.1155/2014/492832
5. Rahman, M. A., Islam, M. T., Singh, M. S. J., Samsuzzaman Md., and Chowdhury, M. E. H., 2021: Synthesis and characterization of Mg–Zn ferrite based fexible microwave composites and its application as SNG metamaterial, Scientific Reports, 11, 7654, https://doi.org/10.1038/s41598-021-87100-6

 doi:10.20944/preprints202403.1642.v2

6. Ramanjaneyulu, K., Suryanarayana, B., Raghavendra, V., Murali, N., Parajuli, D. and Chandramouli, K., 2021: Synthesis, microstructural and magnetic properties of Cu doped Mg0.5Zn0.5Fe2O4 ferrites, Solid State Technology, 64(2),7192-7200, http://solidstatetechnology.us/index.php/JSST/article/view/10932
7. Varma, P. P., Suryanarayana, B., Raghavendra, V., Parajuli, D., Murali, N. and Chandramouli, K., 2020: Effect of Cr Substitution on Magnetic Properties of Co-Cu Nano Ferrites, Solid State Technology, 63(5), 8820-8827, http://solidstatetechnology.us/index.php/JSST/article/view/7828
8. Balavijayalakshmi, J., Sudha, T., & Karthika, K. (2015). Investigation on structural and magnetic properties of cobalt doped magnesium ferrite nanoparticles.
9. Ma, D., Lu, J., Fang, X., Yang, K., Wang, K., Zhang, N., Han, B., & Ding, M. (2021). Parameter Modeling Analysis of a Cylindrical Ferrite Magnetic Shield to Reduce Magnetic Noise. IEEE Transactions on Industrial Electronics, 69, 991-998. https://doi.org/10.1109/TIE.2021.3050351.
10. Samir, A., Wang, J., & Fujiwara, O. (2000). A Practical Approach for Estimation of Load Effect Produced by Ferrite Core Attached to Wire above a Ground Plane. Ieej Transactions on Electronics, Information and Systems, 120, 8-13. https://doi.org/10.1541/IEEJEISS1987.120.1_8.
11. Tsui, F. (1962). Improving the Performance of the Sense-Amplifier Circuit Through Pre-Amplification Strobing and Noise-Matched Clipping. IRE Transactions on Electron. Comput., 11, 677-683. https://doi.org/10.1109/TEC.1962.5219430.
12. Miyashita, T., Nitta, S., & Mutoh, A. (1998). Prediction of noise reduction effect of ferrite beads on electromagnetic emission from a digital PCB. 1998 IEEE EMC Symposium. International Symposium on Electromagnetic Compatibility. Symposium Record (Cat. No.98CH36253), 2, 866-871 vol.2. https://doi.org/10.1109/ISEMC.1998.750321.
13. Samir, A., & Fujiwara, O. (1999). Calculation of load effect produced by ferrite core attached to wire above a ground plane. 1999 Asia Pacific Microwave Conference. APMC'99. Microwaves Enter the 21st Century. Conference Proceedings (Cat. No.99TH8473), 1, 182-185 vol.1. https://doi.org/10.1109/APMC.1999.828080.
14. Schneider, C. A., Rasband, W.S., Eliceiri, K.W., 2012: NIH Image to ImageJ: 25 years of image analysis, Nature Methods, 9, 671–675, https://doi.org/10.1038/nmeth.2089
15. Abraham, A. G., Manikandan, A., Manikandan, E., Vadivel, S., Jaganathan, S. K., Baykal, A. and Renganathan, P. S., 2018: Enhanced magneto-optical and photo-catalytic properties of transition metal cobalt (Co2+ ions) doped spinel MgFe2O4 ferrite nanocomposites, Journal of Magnetism and Magnetic Materials, 452, 380-388, https://doi.org/10.1016/j.jmmm.2018.01.001
16. Kumar, S. R., Priya, G. V., Aruna, B., Raju, M. K., Parajuli, D., Murali, N., Verma, R., Batoo, K. M., Kumar, R. and Narayana, P. L., 2022: Influence of Nd3+ substituted Co0.5Ni0.5Fe2O4 ferrite on structural, morphological, dc electrical resistivity and magnetic properties, Inorganic Chemistry Communications, 136, 109132, https://doi.org/10.1016/j.inoche.2021.109132
17. Shao, L., Sun, A., Zhang, Y., Yu, L., Suo, N. and Zuo, Z., 2021: Comparative study on the structure and magnetic properties of Ni-Mg-Co ferrite doped with Al and rare earth elements, Journal of Materials Science: Materials in Electronics, 32(5), 5339-5352, https://doi.org/10.1007/s10854-020-05161-1
18. Shafiee, S., Arab, A. and Riahi-Nouri, N., 2021: Enhanced magnetic permeability in Ni1−x(Zn0.6Mg0.2Cu0.2)xFe2O4 synthesized by auto combustion method, Bulletin of Materials Science, 44(2), 1-9, https://doi.org/10.1007/s12034-021-02429-y
19. Garg, A. and Pal, D., 2021: Inferring metal binding sites in flexible regions of proteins, Proteins: Structure, Function, and Bioinformatics, 89(9), 1125-1133, https://doi.org/10.1002/prot.26085
20. Monisha, P., Priyadharshini, P., Gomathi, S. S. and Pushpanathan, K., 2021: Ferro to superparamagnetic transition: Outcome of Ni doping in polyethylene glycol capped CoFe2O4 nanoparticles, Journal of Alloys and Compounds, 856, 157447, https://doi.org/10.1016/j.jallcom.2020.157447
21. Komali, C., Murali, N., Parajuli, D., Ramakrishna, A., Ramakrishna, Y. and Chandramouli, K., 2021: Effect of Cu2+ substitution on structure, morphology, and magnetic properties of Mg-Zn spinel ferrite, Indian Journal of Science and Technology, 14(27), 2309-2316, https://doi.org/10.17485/IJST/v14i27.527
22. Hankare, P. P., Patil, R. P., Jadhav, A.V., Pandav, R. S., Garadkar, K. M., Sasikala, R. and Tripathi, A. K., 2011: Synthesis and characterization of nanocrystalline Ti-substituted Zn ferrite, Journal of Alloys and Compounds, 509, 2160-2163, https://doi.org/10.1016/j.jallcom.2010.10.173
23. Thorat, L. M., Patil, J. Y., Nadargi, D. Y., Ghodake, U. R., Kambale, R. C. and Suryavanshi, S. S., 2018: Co2+ substituted Mg–Cu–Zn ferrite: Evaluation of structural, magnetic, and electromagnetic properties, Journal of Advanced Ceramics, 7(3), 207-217, https://doi.org/10.1007/s40145-018-0272-6

24. Hoyos-Sifuentes, D. H., Resendiz-Hernandez, P. J., Diaz-Guillen, J. A., Ochoa-Palacios, R. M. and, Altamirano-Guerrero, G., 2022: Synthesis and characterization of MgFe2O4 nanoparticles and PEG-coated MgFe2O4 nanocomposite, Journal of Materials Research and Technology, 18, 3130-3142,https://doi.org/10.1016/j.jmrt.2022.03.117
25. Balavijayalakshmi, J., and Sudha, T., 2017: Effect of Cobalt Substitution on Structural and Magnetic Properties of Magnesium Ferrite Nanoparticles. In: Ebenezar, J. (eds) Recent Trends in Materials Science and Applications,Springer Proceedings in Physics, 189, 289-297, https://doi.org/10.1007/978-3-319-44890-9_27
26. Xavier, S., Thankachan, S., Jacob, B. P. and Mohammed, E. M., 2013: Effect of sintering temperature on the structural and magnetic properties of cobalt ferrite nanoparticles, Nanosystems: Physics; Chemistry; Mathematics, 4(3), 430–437, https://cyberleninka.ru/article/n/effect-of-sintering-temperature-on-the-structural-and-magnetic-properties-of-cobalt-ferrite-nanoparticles
27. Vergis, B. R., Kottam, N., Krishna, R. H., and Kumar, G. A., 2021: Comparison of magnetic and dielectric properties of transition metal nanospinel ferrites, MFe2O4, (M = Co, Cu, Ni, Zn) synthesized by one-pot combustion route, Materials Today: Proceedings, 49, 870-877, https://doi.org/10.1016/j.matpr.2021.06.177
28. Bharathi R. V., Raju M. K., Uppugalla S., Raghavendra V., Parajuli D., Suryanarayana B., Mulushoa S. Y., Murali N., and Samatha K., 2023: Cu2+ substituted Mg-Co ferrite has improved dc electrical resistivity and magnetic properties, Inorganic Chemistry Communications, 149, 110452, https://doi.org/10.1016/j.inoche.2023.110452
29. Kaiser, M., Hashhash, A. and Hassan, H. E., 2021: Dielectric behavior and complex impedance analysis of Ti-doped Mg0.5Cu0.5Mn0.4Fe1.6O4 ferrites, Applied Physics A, 127(3), 1-13, https://doi.org/10.1007/s00339-021-04318-x
30. Parajuli, D., Murali, N., Rao A. V., Ramakrishna, A., Mulushoa S, Y., Samatha, K., 2022: Structural, dc electrical resistivity and magnetic investigation of Mg, Ni, and Zn substituted Co-Cu nano spinel ferrites, South African Journal of Chemical Engineering, 42, 106-114, https://doi.org/10.1016/j.sajce.2022.07.009